Pergamon

Geochimica et Cosmochimica Acta, Vol. 68, No. 4, pp. 701–714, 2004

0016-7037/04 $30.00 + .00

doi:10.1016/S0016-7037(03)00499-X

Pyrite oxidation in moist air

JEANETTE K. JERZ and J. DONALD RIMSTIDT*

Department of Geological Sciences, Virginia Polytechnic Institute and State University, 4044 Derring Hall, Blacksburg, VA 24061 USA

(*Received July* 10, 2002; *accepted in revised form May* 28, 2003)

Abstract—The rate of pyrite oxidation in moist air was determined by measuring, over time, the pressure difference between a sealed chamber containing pyrite plus oxygen and a control. The experiments carried out at 25°C, 96.7% fixed relative humidity, and oxygen partial pressures of 0.21, 0.61, and 1.00 atm showed that the rate of oxygen consumption is a function of oxygen partial pressure and time. The rates of oxygen consumption (r, mol/m^{2}sec) fit the expression

$$\frac{dn}{dt} = 10^{-6.6} P^{0.5} t^{-0.5} \quad \text{(A)}$$

where P is the partial pressure of oxygen (atm) and t is time (sec). It appears that the rate slows with time because a thin layer of ferrous sulfate + sulfuric acid solution grows on the pyrite and retards oxygen transport to the pyrite surface. At very short reaction times, the rate of pyrite oxidation in air is slightly faster than the aqueous oxidation rate at the same oxygen partial pressure and temperature. At greater extents of reaction, the rate slows significantly and approaches the rates reported by humidity cell studies. This slower rate of oxidation in air appears to be more appropriate than the aqueous oxidation rate for modeling pyrite oxidation in unsaturated waste piles. At relative humidity less than 95%, a solid ferrous sulfate phase (melanterite or szolmonokite) becomes saturated and will precipitate from the ferrous sulfate + sulfuric acid solution in cracks and on the pyrite surface. These solids have the potential to wedge apart the sample leading to physical disaggregation of the pyrite as is often seen in museum samples.

1. INTRODUCTION

The oxidation of pyrite at or near the earth's surface creates acidic, metal-rich solutions that can have a seriously negative impact on the biota and quality of nearby receiving waters (Smith and Huyck, 1999; Kelly, 1999). For this reason, much effort has gone into studying pyrite oxidation to understand the chemistry of the process with the goal of reducing its impact. Plumlee and Logsdon (1999) have presented an excellent recent review of the chemical, physical, and biologic processes involved in acid mine drainage.

There have been several studies of the rate of pyrite oxidation under subaqueous conditions (Williamson and Rimstidt, 1994 and references within). However, pyrite exists frequently in unsaturated waste piles where it oxidizes subaerialy. Ritchie (1994), Elberling et al. (1994) and Elberling and Nicholson (1996) have developed models that consider the air oxidation of pyrite in waste piles. They assumed that the rates are limited by oxygen diffusion through the wastes. We have developed a method of measuring the rate of pyrite oxidation in humid air as a function of oxygen partial pressure that allows a quantitative determination of the rate of the chemical reaction that occurs at the pyrite surface.

Anecdotal evidence for significant rates of pyrite oxidation in humid air comes from museum curators who have found that pyrite samples often crumble during storage (Howie, 1992). Curators, concerned with the preservation of their samples, refer to this process as "pyrite disease" and great care is taken to minimize the damaging effects. This includes keeping the samples in low humidity environments, coating the samples with clear resins that act as protective barriers to oxygen and water, and removing the products of oxidation (Bannister, 1933; Bannister, 1937). While these efforts may be cost effective for rare and expensive museum samples, they are impractical at a field scale where pyrite grains in waste piles oxidize in a similar manner to untreated museum samples.

The few studies that have determine the rates of pyrite oxidation in air are listed in Table 1. Morth and Smith (1966) published the results of Birle (1963) and Kim (1964) who used Warburg manometry, described by Umbreit et al. (1972), to study the rate of oxygen consumption due to pyrite oxidation in vapor as a function of relative humidity, oxygen pressure, and temperature. They report a constant rate over long time periods (several days to weeks). At 25°C and 96% relative humidity, this rate is $10^{-7.23}$ (mol O_2/m^{2}sec) in 100% oxygen and $10^{-7.66}$ (mol O_2/m^{2}sec) in air (21% oxygen). Morth and Smith (1966) found "significantly faster rates when pyrite oxidizes in air as compared to solution." They concluded that the reaction order of oxygen was fractional and the rate-limiting step of pyrite oxidation was the physical adsorption of dissociated oxygen on the surface of pyrite. We are unaware of any other study in which the authors directly measured oxygen consumption and controlled humidity.

Many studies of pyrite oxidation in air have used humidity cells. Note that humidity cell experiments, which use flooded then drained columns of pyritic material to estimate the rate of pyrite oxidation in mine wastes, probably measure a mixed rate that includes pyrite oxidation in air, pyrite oxidation in solution, and transport of oxygen. This method calls for the saturation of the sample with water, which is later drained, to create

* Author to whom correspondence should be addressed (jdr02@vt.edu).

Table 1. Oxidation rate of pyrite in humid air reported by other authors (recalculated from Hammack and Watzlaf, 1990). Morth and Smith (1966) used oxygen consumption as the rate-determining variable, other authors used humidity cells and monitored sulfate production to determine the rate of pyrite oxidation.

Study	Rate (mol O_2/m^2sec)	T (°C)	O_2 Dependence	Species Monitored
Morth and Smith (1966)*	$10^{-7.7}$ in air $10^{-7.2}$ in 100% O_2	25	Fractional order	Oxygen
Brayley (1960)	$10^{-6.5}$ in air	N/A	First order	Sulfate
Rogowski and Pionke (1984)	$10^{-7.4}$ in air	25	Not determined	Sulfate
Nicholson et al. (1988)	$10^{-8.7}$ in air	23	Fractional order	Sulfate
Hammack & Watzlaf (1990)	$10^{-5.7}$ surface rate $10^{-8.7}$ bulk rate	25	0th order >10% 1st order > 5%	Sulfate
This study	$10^{-7.0}$ initial rate in air	25	0.5 order	Oxygen

* Includes data from two unpublished M.S. theses (Birle, 1963 and Kim, 1964).

a partially saturated mass with a humid environment. It is likely that liquid water is still present in the pore spaces between some of the grains and as a coating on the grains' surfaces. Although oxygen partial pressure and temperature can be controlled in these experiments, relative humidity is not. Extraction of pyrite oxidation rate data is difficult because the activity of water varies over the course of an experiment. Although the rates generated by the Morth and Smith (1966) and those from humidity cells cannot be compared directly, they provide useful reference values. The rates reported by humidity cell studies range between $10^{-6.5}$ and $10^{-8.7}$ mol O_2/m^2sec (Table 1).

Borek (1994) investigated pyrite oxidation in the vapor phase using both hydrothermal and sedimentary pyrite samples, but did not report a rate law. This study provides helpful information about the products generated by pyrite oxidation in humid air. Borek (1994) found that liquid water condensed on certain types of pyrite at relative humidity greater than 70%. In addition, ferrous sulfate salts ($FeSO_4 \cdot nH_2O$; n = 7 for melanterite; n = 4 for rozenite; n = 1 for szomolnokite) and hematite were detected using Mössbauer spectroscopy as reaction products on pyrite samples that had oxidized under a range of relative humidity (34%–79%). The type of and amount of reaction product varied with pyrite source but the overall reaction seems to be:

$$FeS_2 + 7/2O_2 + H_2O = FeSO_4 + H_2SO_4 \quad (1)$$

The purpose of this paper is to determine the rate of pyrite oxidation in humid air as a function of oxygen partial pressure. The findings of this study will connect those studies that investigated very short extents of pyrite reaction using X-ray photon spectroscopy (XPS) studies (Nesbitt and Muir, 1994; Knipe et al., 1995; Nesbitt et al., 1998; Guevremont et al., 1998a; Guevremont et al., 1998b; Elsetinow et al., 2000; Nesbitt et al., 2000) with the longer-term humidity cell studies.

2. MATERIAL AND METHODS

2.1. Run Materials

Coarse-grained pyrite from Peru was used in all experiments. This is the same pyrite that was used in the experiments reported by Williamson and Rimstidt (1994). It contains no calcite and minor fluorite. The samples were hand picked to remove the fluorite. The pyrite was crushed and sieved to recover the 40–60-mesh size. The specific surface area of these grains was too low to determine reliably by BET surface area analysis. Foust et al. (1980) provides a graph that shows the relationship between surface area and grain size, which we used to estimate that the specific surface area of the pyrite used in each experiment was 0.01 m^2/g. The pyrite was washed with ethyl alcohol three to five times until the supernatant was clear. The samples were then sonicated in ethyl alcohol to removed adhering fine particles and dismember any bacteria. This procedure was repeated at least three times until the supernatant was clear. The grains were dried at 70°C for 12 h. This method of sample preparation produced predominantly freshly fractured surfaces, similar to those found in tailings. After cleaning, 5.1 g aliquots of pyrite were placed in glass ampoules that were evacuated and sealed. The pyrite was stored at room temperature in the evacuated ampoules until use.

2.2. Reactor Design

The rate of oxygen consumption by a pyrite sample was measured using a modified Barcroft apparatus. Barcroft manometry has been used extensively by biologists to determine respiration rates (Umbreit et al., 1972). The design of our system is shown in Figure 1. The apparatus consists of two chambers joined by a manometer. The chambers are sealed during an experiment and the pressure change in one chamber relative to the other is documented by a change in oil height in the arms of the manometer. The reaction chamber (right) holds the pyrite and the control chamber (left) containing quartz is used as a pressure reference so that once the chambers are sealed changes in external (atmospheric) pressure do not affect the measurements. During an experiment, 2.65 g of quartz, which occupies the same volume as the pyrite used in the experiment, is placed in the control chamber so that the volumes of the two chambers are equal. The manometer is made from a 300 mm long, 0.5 mm I.D. glass tube that was bent into the shape of the letter U. It is approximately half filled with oil that contains a red dye that makes it easily visible. The oil has a density of 0.869 g/mL. This fluid is approximately 15 times less dense, and therefore approximately 15 times more sensitive to pressure change, than mercury. Pressure measurements are made by measuring the difference in height (in mm) between the oil levels in the two arms of the manometer. With this manometer, we are able to measure pressure differences on the order of 8.4×10^{-5} atm. This translates into changes due to the consumption of as little as 1×10^{-7} moles of oxygen. Vinyl tubes are secured to the end of each arm of the manometer with metal ties and then attached to the reaction and control chambers with Luer lock fittings that attach to a stopcock.

The acrylic chambers are cylindrical with a total volume of 28.96 cm^3 (Fig. 2). At the top of each chamber are two holes that are sealed with silicone rubber. One is used as a septum that is used to withdraw gas samples for calibration purposes. The other holds a glass funnel that is used to place the minerals into the chambers and can be sealed with a silicon rubber stopper. On the side of each chamber is a threaded port that accepts a NPT fitting that attaches to a 3-way stopcock. One position opens to the chamber, the second opens to the manometer, and the third opens to the gas source. The manometer and the gas source are attached to tubing that attaches to the stopcock with Luer fittings. Inside each chamber is a sample holder that is supported by an internal ledge.

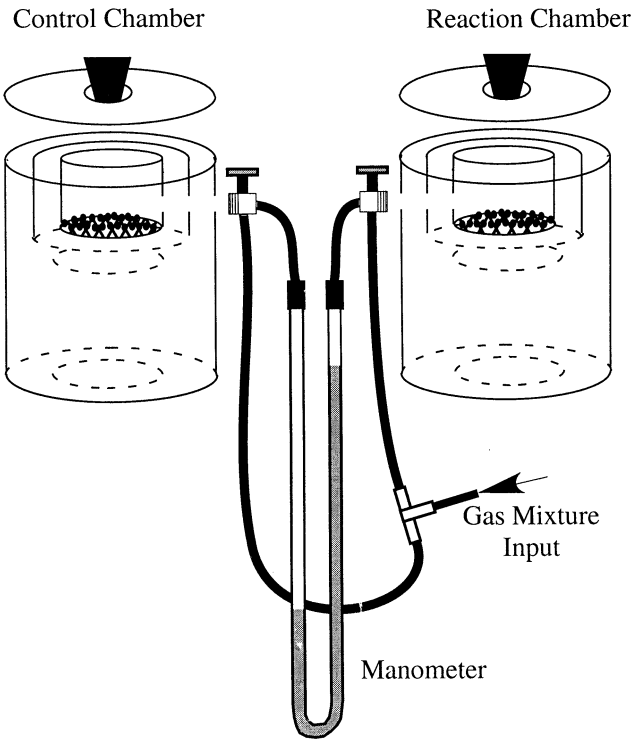

Fig. 1. Modified Barcroft apparatus used in pyrite oxidation experiments. The reactor consists of two chambers connected by a manometer filled with oil. The reaction chamber (right) holds pyrite and the control chamber (left) is used as a pressure reference throughout the experiment. The manometer is attached to each chamber via a stopcock. The partial pressure of oxygen is controlled with gas mixtures of known oxygen content. before each experiment, the gas flows from a tank through a gas wash bottle and copper coil into a tee that splits the gas flow into the chambers through the stopcocks. During the experiments, the stopcocks are closed and the chambers are sealed. The manometer responds to change in pressure due to oxygen consumption by pyrite oxidation.

The holder is a 1.3 cm high by 3.12 cm diameter acrylic ring with 0.32 cm thick walls. Nylon mesh glued to the bottom of the ring supports the sample.

The initial partial pressure of oxygen inside the reactors is set by flowing a gas mixture (O_2-N_2) of known oxygen content through in each chamber. It enters through the 3-way stopcock and exits through the sample funnel. For the $P_{O_2} = 0.21$ experiments, the chambers were flushed with air. A 60.6% O_2 (balance N_2) mixtures was used to set the $P_{O_2} = 0.61$ atm and pure oxygen was used to set the $P_{O_2} = 1.0$ atm. To adjust the gas to the relative humidity and temperature of the experiment, the gas flowed from the tank through a gas wash bottle containing a 1.0 m NaCl solution with a $a_{H_2O} = 0.967$ (Robinson and Stokes, 1959) and then through a copper coil immersed in the same constant temperature bath that contained the experiment. The output from the copper coil is split with a reducing tee-junction. The two gas streams then flowed through the Luer fittings that are attached to the stopcocks of each chamber.

The gas-wash bottle, chambers, the stopcocks, and all connections except to the manometer are completely immersed in a 25°C water bath during the experiments. The chambers are supported in the bath by an acrylic stand. The manometer is attached to the reactor stand immediately outside the bath.

2.3. Experimental Procedure

Experiments were performed at 25±1°C, 96.7% relative humidity, and P_{O_2} values of 0.21, 0.60, and 1.00. Each chamber was filled with 18.00 mL of a 1.0 m NaCl solution that controls relative humidity at 96.7% (Robinson and Stokes, 1959). Once filled, the chambers have a headspace of approximately 10 cm^3.

The apparatus is sensitive to even very small pressure leaks. To assure that none were present, prior each experiment, the chambers were sealed and the stopcocks were opened to allow gas to flow in from the tank. The chambers were pressurized to 5 psi and all joints observed for between 6 and 12 h. If gas bubbles appeared, the chamber was removed and resealed. The apparatus was pressure-tested again after each experiment to assure that leaks had not developed during the experiment.

At the beginning of each experiment the reactors were assembled and the stopcocks opened to allow pressure to equalize between each chamber, the atmosphere, and the gas source. The chambers and manometer were secured to the reactor stand and it was placed in the constant temperature bath. Sealed pyrite ampoules and a test tube containing quartz for the control chamber were also immersed in the bath. All parts of the system remained in the constant temperature bath for 12 h so they came to thermal equilibrium before an experiment was started.

After the apparatus was thermally equilibrated, quartz sand was poured through the funnel in the control chamber and the regulator on the gas tank was turned down to 1 psi so that there was a small amount of positive pressure to prevent back flow of air into the headspace of the chambers. The pyrite ampoule was opened and pyrite was immediately poured into reaction chamber. Each sample funnel was sealed with a silicone stopper that was held in place by a Teflon screw. The gas source to the chambers was closed, first the reaction chamber and then the control, and the timer was started marking the beginning of the experiment. Both chambers were then fully immersed in the bath.

As pyrite oxidation consumed oxygen, the pressure inside the reaction chamber decreased and the oil in that arm of the manometer rose. During the experiment, time, the difference in oil height (in mm), bath temperature, room temperature, and atmospheric pressure were recorded. The experiment was stopped when the oil level in the reactor arm reached the top of the manometer. Thus, all experiments proceeded to approximately the same extent of reaction. Four or five duplicate experiments were performed at each partial pressure of oxygen. Experiments were numbered sequentially, regardless of initial oxygen pressure. Several experiments failed, usually due to leaks, and their results are not reported in the data table.

The volume/pressure relationship of the reactor was calibrated after each experiment by extracting known volumes of gas from the reaction chamber with a gas syringe and measuring the corresponding change in oil height in the manometer. The ideal gas law was used to calculate the number of moles of oxygen that correspond to this volume. The relationship between the number of moles of oxygen in a volume of gas removed from the chambers and the corresponding change in pressure (measured in mm of oil height) was used to generate a calibration constant that was used to convert raw data (mm of oil height) into moles of oxygen consumed at each time measurement. The calibration procedure was done after each experiment to account for the small changes in headspace that may result from different chambers and manometers.

The concentration of oxygen (mol/m^3) in the reaction chamber at each time was determined by subtracting the number of moles of oxygen consumed divided by the headspace in the chambers (~10 cm^3) from the initial oxygen concentration in the gas phase. These values were converted to partial pressure of oxygen using the ideal gas law.

After reactor calibration, the chambers were opened and the samples were removed. The quartz was discarded and the pyrite was preserved in a glass jar in a dessicator for later analyses with Field Emission Scanning Electron Microscopy (FESEM) and Energy Dispersive Spectroscopy (EDS).

2.4. Rate Calculation

The experimental data are reported as of moles of oxygen consumed (n, moles) versus time (t, seconds). The rate of reaction for each duplicate experiment was determined by numerical differentiation of these data. Preliminary analysis of the data showed that they approximately fit a power law of the form:

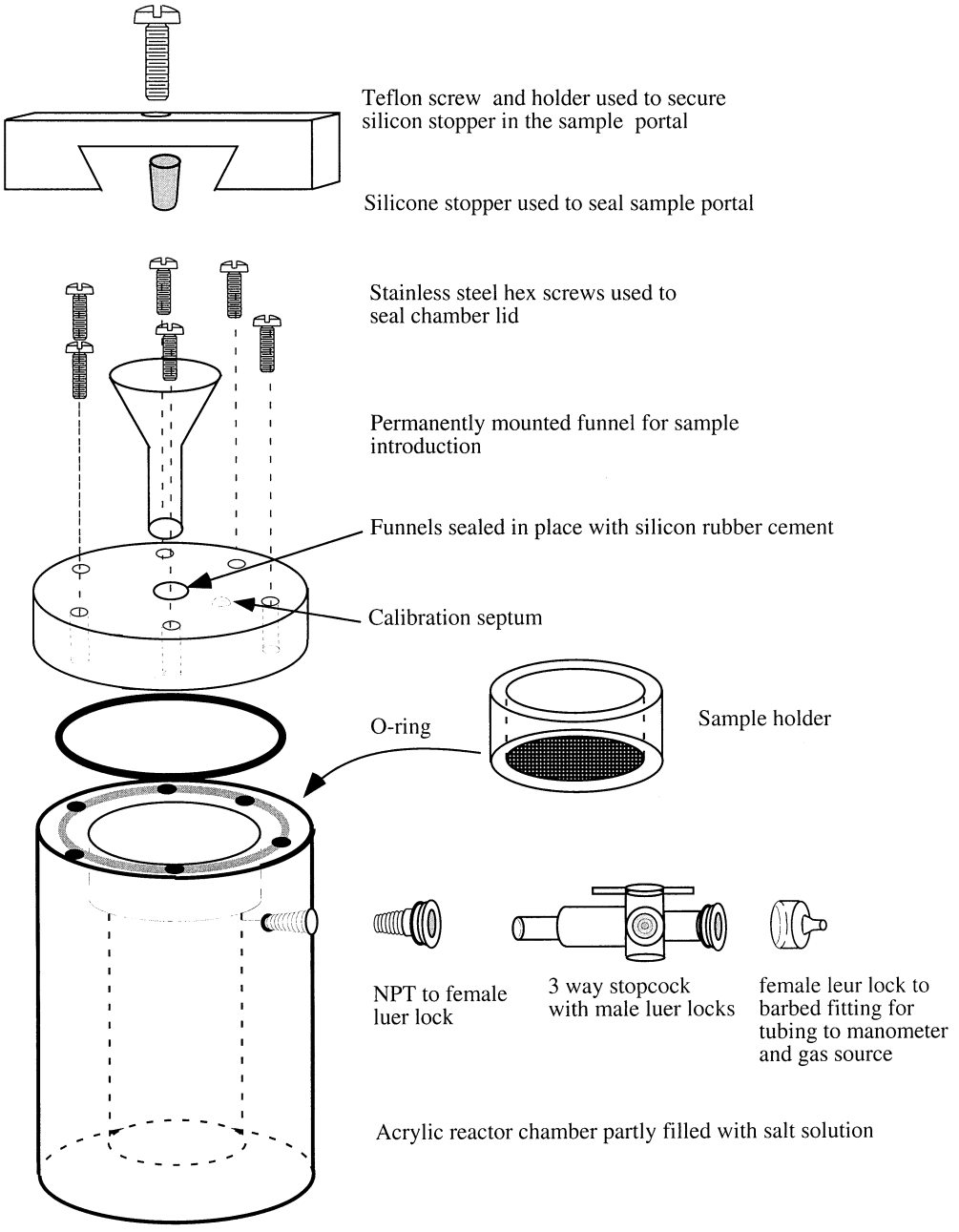

Fig. 2. Diagram of reaction and control chamber assembly. The parts are drawn to scale and the outside diameter of the reactor is 5 cm.

$$n = kt^{0.5} \tag{2}$$

(Fig. 3). By taking the derivative of Eqn. 2, the rate could be estimated with an equation of the form

$$r = \frac{dn}{dt} = \frac{k}{2t^{0.5}} \tag{3}$$

The rate, r_o at each data point (n_0, t_0) was estimated by calculating the slope of the line between the data points prior (n_{-1}, t_{-1}) and following (n_{+1}, t_{+1}):

$$slope(n_0,t_0) = \frac{n_{+1} - n_{-1}}{t_{+1}^{0.5} - t_{-1}^{0.5}}. \tag{4}$$

The slope, which is equal to the rate constant divided by 2, was substituted into Eqn. 3 to find the rate at each time using the equation:

$$r_0 = \frac{slope}{t_0^{0.5}}. \tag{5}$$

Negative rates were discarded. These numerically determined rates were used to develop the rate models, discussed later.

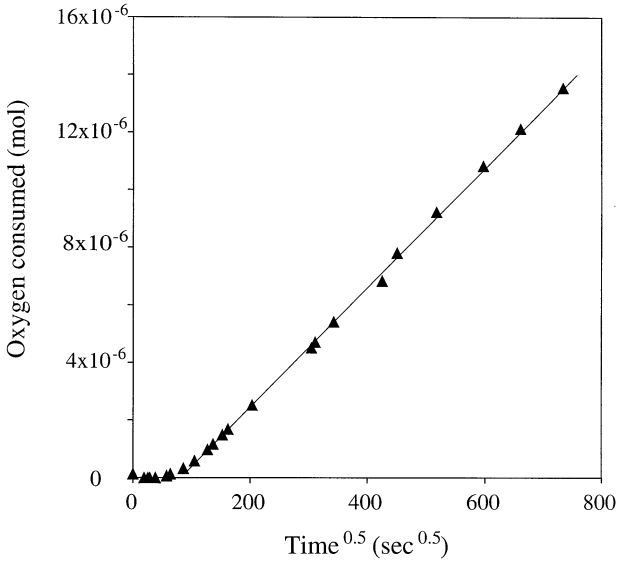

Fig. 3. Data from experiment PY 43 plotted against the square root of time. The number of moles of oxygen consumed is a linear function of the square root of time over most of the reaction time.

3. RESULTS

The results of the pyrite oxidation experiments are tabulated in Appendix 1 and shown in Figure 4. The duplicate experiments are represented as different symbols on the graphs at each partial pressure of oxygen.

The numerically determined rates of oxygen consumption at each partial pressure of oxygen (see Appendix) are shown in Figure 5. The rates slow by approximately two orders of magnitude over the course of each experiment. Oxygen was consumed fastest in the 100% P_{O_2} experiments, and slowest in the 21% P_{O_2} experiments. Note that these results show that log r is a linear function of log t and the slopes of these lines are approximately -0.5.

The pyrite grains adhered together in small clumps when they were removed from the chamber after the experiment. This observation is consistent with the idea that a solution had formed on the surfaces during oxidation and the surface tension of that solution caused the clumping. Field Emission Scanning Electron Microscopy (FESEM) was used to observe dried surfaces of the reacted pyrite grains. Figure 6 shows the anhedral to subhedral crystals that formed by the rapid evaporation of the solution when the pyrite grains were placed in the storage dessicator. Iron and sulfur were identified in the salts using energy dispersive spectroscopy (EDS), which we interpret to mean that the crystals are iron sulfates that formed from an evaporating ferrous sulfate + sulfuric acid solution. This result is consistent with the observations of Borek (1994) and Todd et al. (2003) who also report the presence of iron sulfates on the surfaces of air-oxidized pyrite samples.

4. DISCUSSION

4.1. Solution Film Formation

Our experimental results show that the rate of oxygen consumption by pyrite is a function of time and oxygen partial pressure. The rate at which oxygen was consumed slowed with time and the rates of reaction increased as the partial pressure of oxygen increased. Our objective is to develop a rate law that is consistent with a physical model and the overall chemical reaction.

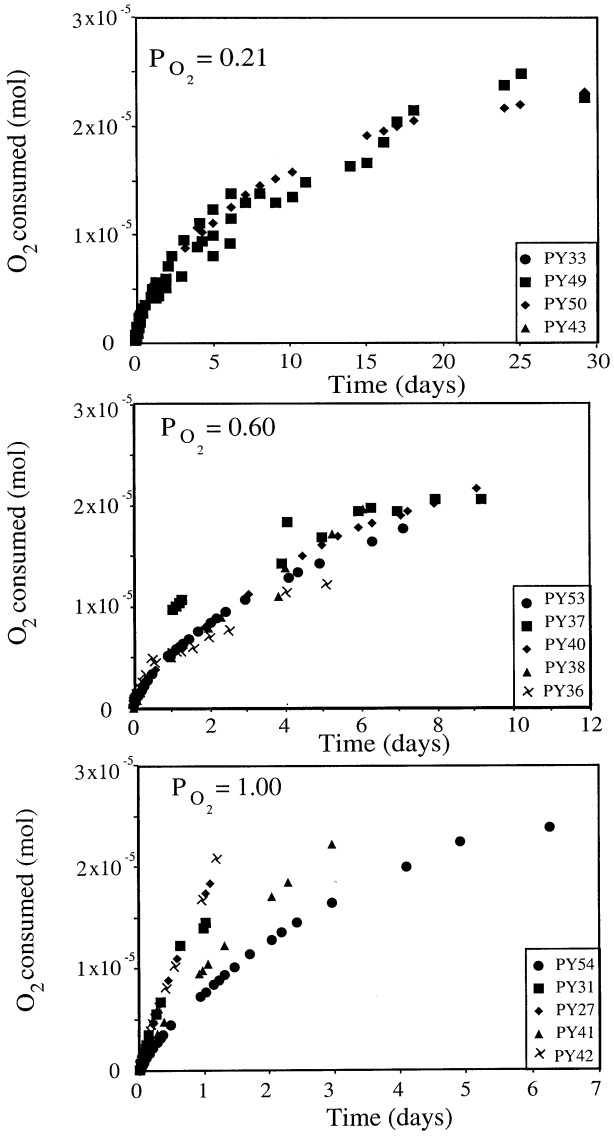

Fig. 4. Graphs of moles of oxygen consumed versus time at each oxygen partial pressure. Replicate experiments at the same pressure are shown by different symbols. Note that although the y-axes of these three graphs are the same the x-axes are different. The shorter time span for the bottom graph pulls the data points apart and gives the false impression that there is more scatter in those data. The original data are tabulated in Appendix I.

The development of a thin film of solution on the surface of the oxidizing pyrite grains is an important physical process that we must consider. The film is too thin to be seen visually, but we conclude that it must be present because its surface tension caused the reacted pyrite grains to adhere together in small clusters after reaction. In addition, we observed iron sulfate salts that had developed and crystallized on reacted pyrite surfaces after the solution evaporated. Borek (1994) reported a

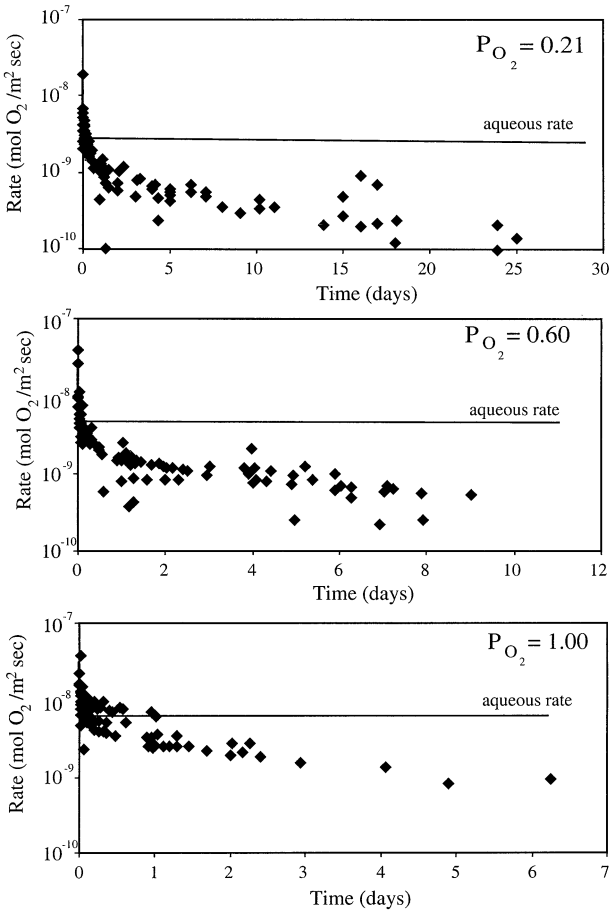

Fig. 5. Graphs of the numerically determined rate of oxygen consumption versus time. Data from replicate experiments have been pooled. The values for the rate at each measurement are listed in Appendix I. The solid line is the rate of pyrite oxidation in aqueous solutions calculated from Williamson and Rimstidt (1994).

similar wetting of pyrite grains oxidized in moist air. We believe that this solution develops due to the hygroscopic nature of the ferrous sulfate and sulfuric acid reaction products (Eqn. 1).

The thickness of the solution film was estimated by calculating the number of moles of ferrous sulfate and sulfuric that are produced per mole of pyrite oxidized and then using the properties of ferrous sulfate + sulfuric acid solutions to estimate the amount of water that would be absorbed from the surrounding vapor phase. For every 3.5 mol of oxygen consumed by pyrite, 1 mol of ferrous sulfate and 1 mol of sulfuric acid are produced (Eqn. 1). Ferrous sulfate and sulfuric acid are hygroscopic and react with the water in vapor phase, which was buffered by the sodium chloride solution at 96.7% relative humidity. We used Pitzer equations (Jerz, 2002) to calculate the concentration of an equal molar ferrous sulfate + sulfuric acid solution in equilibrium with this relative humidity (approximately 0.5 m). To maintain a 0.5 m concentration, the reactants must absorb 2 kg (approximately 2 L) of water from the atmosphere for every mole of pyrite oxidized or 0.572 kg for every mole of oxygen consumed. Spread over 1 m^2 of pyrite surface, the thickness of a solution film produced by this water absorption is 5.72×10^{-5} m/mol O_2 consumed. Therefore, the layer thickness (L) at any extent of reaction can be expressed as the thickness constant (k_l) (5.72×10^{-5} m/mol) multiplied by the number of moles of oxygen consumed.

$$L = k_l n \tag{6}$$

We estimated the solubility of oxygen in a ferrous sulfate + sulfuric acid solution using the methods of Tromans (2000), who developed an empirical function for the solubility of oxygen as a function of solute concentration. The function can be used to determine an apparent Henry's law constant for the solution that formed in our experiments. Although Tromans (2000) did not determine empirical constants for ferrous sulfate

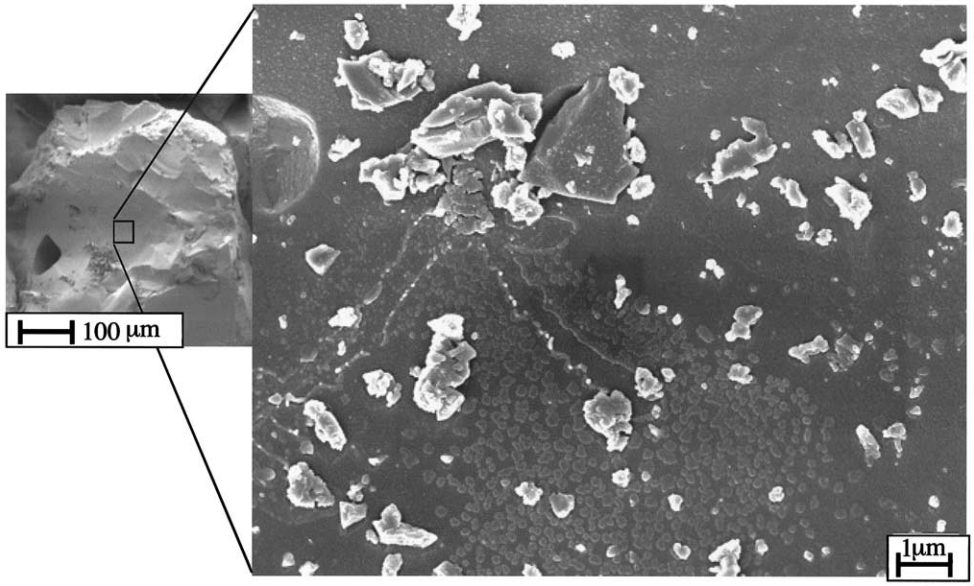

Fig. 6. FESEM image of pyrite surface after oxidation in humid air. The precipitates contained iron and sulfur as determined by EDS.

+ sulfuric acid solutions, he did determine them for magnesium sulfate, copper sulfate, and sodium sulfate. The apparent Henry's law constants of 0.5 m solution of $MgSO_4$, $CuSO_4$, and Na_2SO_4 are 0.960×10^{-3}, 1.09×10^{-3}, and 0.881×10^{-3}, respectively. We chose to model the solubility of oxygen in ferrous sulfate + sulfuric acid solutions with the average (0.985×10^{-3}) of the K_H' of copper sulfate and sodium sulfate because they represent a 2:2 and 1:2 electrolyte solution. The Henry's Law constant of oxygen in pure water is 1.26×10^{-3}, for comparison (Langmuir, 1997). Using an apparent K_H' we can describe the solubility of oxygen in ferrous sulfate + sulfuric acid solution as a function of oxygen partial pressure.

$$C_a = K_H' P \tag{7}$$

It is important to know the solubility of oxygen in the film because once it forms, it is the source of oxygen for the oxidation reaction.

4.2. Data Analysis

There are several ways to derive an empirical rate law from our data. The simplest is to determine the relationship between the measured rates, the elapsed time, and the oxygen partial pressure:

$$r = aP^b t^c \tag{8}$$

where a is a rate constant, b is the reaction order of oxygen, and c is the power exponent of time. This equation can be linearized by taking the logarithm of both sides.

$$\log r = \log a + b\log P + c\log t. \tag{9}$$

Multilinear regression of the log-transformed rate data was used to determine the approximate values of a (-6.57 ± 0.07), b (0.58 ± 0.06), and c (-0.42 ± 0.01). The log-transformation changes the weighting of the data, so nonlinear regression is normally a better method to estimate a, b, and c. However, with our data set, the nonlinear regression model did not converge.

A disadvantage to these methods is they use numerically differentiated rate values and numerical differentiation magnifies minor errors in the original data. Therefore, we fit our data to a generalized integrated form of Eqn. 8 using nonlinear regression:

$$n = dP^e t^f \tag{10}$$

This method of analysis finds values of both e (0.46 ± 0.02) and f (0.54 ± 0.01) that are very close to 0.5, which is consistent with the heuristic model of a process discussed in the next section. If $e = f = 0.5$, Eqn. 10 can be recast to

$$d = \frac{n}{P^{0.5}t^{0.5}} \tag{11}$$

to find a value of d for each measurement. Computed values of d range from 13.3×10^{-7} to 0.56×10^{-7} with a mean value of $5.49(\pm0.13)\times10^{-7}$ (Fig. 7). We believe that the best description of the data is given by

$$n = 10^{-6.3}P^{0.5}t^{0.5}, \tag{12}$$

which can be differentiated to find the rate

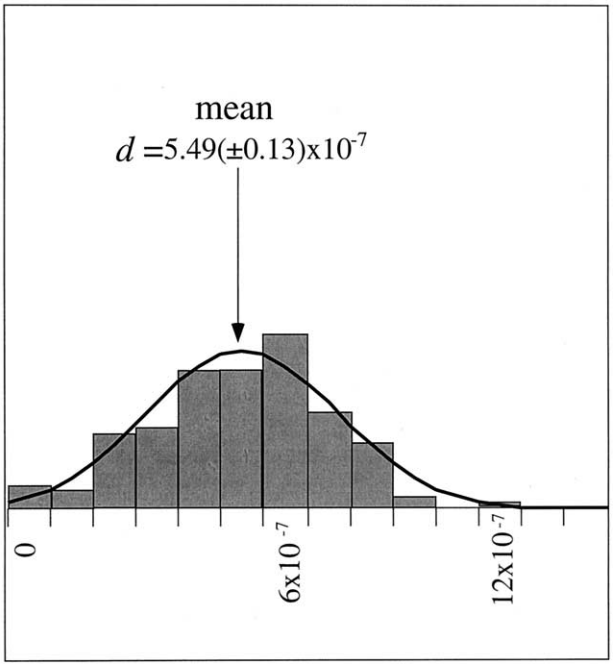

Fig. 7. Distribution of the values of d (see Eqn. 11) calculated from the slope at each datum.

$$r = \frac{dn}{dt} = \frac{10^{-6.6}P^{0.5}}{t^{0.5}}. \tag{13}$$

4.3. Factors that do not Explain the Results

The rate was observed to slow with time at all partial pressures of oxygen. We considered a number of hypotheses to determine what might cause this decrease in rate. These factors are potential explanations for the slowing of the rate, but do not appear to fully explain our results.

The rate does not slow because of the consumption of a monolayer of reactive sites on the surface of pyrite. There are approximately 1×10^{-7} moles of pyrite in one monolayer on 0.051 m^2 of exposed pyrite surface used in these experiments. For comparison, at least 1×10^{-5} moles of pyrite were consumed during the experiment. Therefore, if the surface reacted homogenously, approximately 100 monolayers of pyrite were oxidized in the experiment. It is unlikely that the rate slows due to armoring of the pyrite surface by a solid product. The most likely reaction products are iron sulfate minerals or iron oxide minerals. The sulfuric acid produced by pyrite oxidation inhibits the oxidation of ferrous to ferric iron because this rate is slow at low pH (Singer and Stumm, 1970) and the low pH will also prevent the hydrolysis and precipitation of any ferric iron that might form. Using the Singer and Stumm (1970) rate constant for the oxidation of ferrous iron, we calculated that the rate of consumption of oxygen by ferrous iron at the extent of reaction when 2×10^{-5} moles of O_2 (see Fig. 4) have been consumed would be on the order of 10^{-17} mol/m^2sec. This is 8 to 9 orders of magnitude lower than the rate of oxygen consumption that we measured at that time (Fig. 5). In addition, we did not observe a discoloration of the pyrite surface that

would be expected if iron oxyhydroxides had formed. We observed some iron sulfate salts on the surface of dried grains, but extensive areas of the surface were uncoated.

A great deal of attention has gone to the role of microorganisms in pyrite oxidation. Iron oxidizers such as *Thiobacillus ferrooxidans* and *Leptospirillum ferrooxidans* are known to increase pyrite oxidation rates (Nordstrom and Southam, 1997; Schrenk et al., 1998). However, we do not believe that microbes influenced the rates observed in this study for the following reasons. First, great care was taken in the cleaning and preparation of the chambers and pyrite samples to eliminate microbes. This included washing and sonicating everything in ethyl alcohol and drying at 60°C. Furthermore, the samples were stored in evacuated containers before use in the experiments. *T. ferrooxidan* and *L. ferrooxidans* are not known to have a stasis (spore) phase and therefore could not survive this vacuum storage (Staley et al., 1984). Second, the P_{O_2} = 0.61 and 1.00 experiments contained no CO_2, which these species need as their carbon source to grow. Third, if viable bacteria were present and growing in this system, the oxygen consumption rate should increase with time as the microbial population increased rather than decrease as we observed. Finally, we examined the reacted pyrite grains for the presence of bacteria using microscopy. *Thiobacillus ferrooxidans* are know to consume oxygen at a rate of approximately 1.56×10^{-13} mol O_2/cell day (Lau et al., 1970). If the observed rate of oxygen consumption was due to microbes, there would have to be $\sim5\times10^7$ cells present in each experiment, or approximately one in every 10 μm^2. Using FESEM and conventional SEM, we did not observe any bacterial cells. Reacted samples were treated with a fluorescent dye that stains bacteria and observed with a florescent confocal microscope. No bacteria were observed with this method either. Finally, unreacted and reacted pyrite samples were rinsed in deionized water and these solutions were smeared on an plate prepared with Luria-Bertani agar using the method in Gerhardt et al. (1994) to see if bacteria would grow, but no colonies were observed.

The results of aqueous pyrite oxidation studies were presented in Mckibben and Barnes (1986) and Williamson and Rimstidt (1994). The aqueous oxidation rate is a function of oxygen concentration to the one half power but does not contain a time component. Our observed initial rate of reaction is approximately the same as the rates reported from aqueous studies, but these rates diverge with increasing time (Fig. 5). We have corrected for the decrease in partial pressure due to oxygen consumption by pyrite, but even with this correction the aqueous rate model does not fit our data for long reaction times.

4.4. Preferred Model

Our best explanation for why the rate slowed with time in our experiments is that a film of ferrous sulfate + sulfuric acid grew on the surface as oxidation proceeded, and this film inhibited the transport of oxygen to the surface in direct proportion to the film thickness. We have observed that the rate of pyrite oxidation in air closely matches the rate of oxidation in solution at small values of *t*. At longer values of *t*, the rate slows in proportion to the negative square root of time. Based on these behaviors, we believe that the rate of pyrite oxidation in air is a function of oxygen diffusion through a film of ferrous

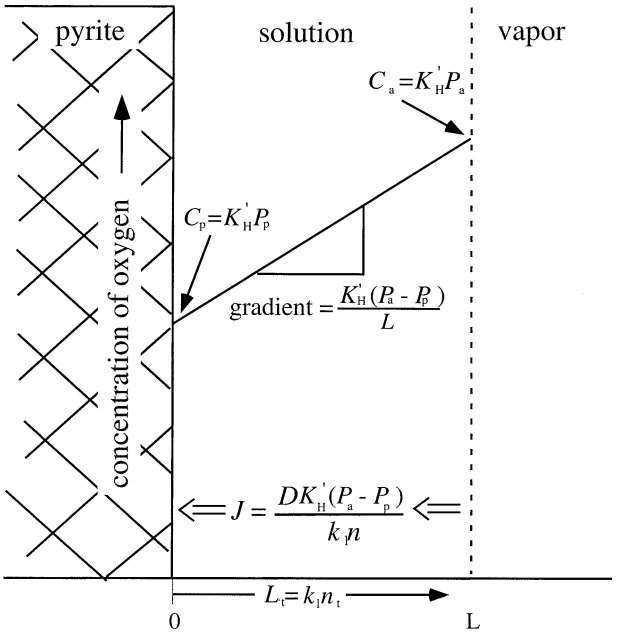

Fig. 8. Physical model of pyrite oxidation in humid air. At steady state, the rate of oxidation is limited by the transport of oxygen through a film of ferrous sulfate + sulfuric acid solution.

sulfate + sulfuric acid solution, which can be described with Fick's first law of diffusion (Crank, 1975)

$$J = \frac{D}{L}(C_a - C_p). \tag{14}$$

At steady state, the flux of oxygen through the film is equal to the observed rate of reaction (Fig. 8). If the rate is transport limited it must be a function of film thickness, which is a function of extent of reaction (Eqn. 6), so

$$\frac{dn}{dt} = J = \frac{D}{k_l n}(C_a - C_p). \tag{15}$$

The concentration of oxygen in the solution at the air interface and at the pyrite surface can be recast to partial pressures with the apparent Henry's law constant. Making this substitution, Eqn. 15 becomes

$$\frac{dn}{dt} = \frac{DK'_H}{k_l n}(P_a - P_p), \tag{16}$$

which can be rearranged to

$$\int n\,dn = \frac{DK'_H}{k_l}(P_a - P_p)\int dt. \tag{17}$$

Integrating Eqn. 17 and solving for n yields the relationship

$$n = \sqrt{\frac{2DK'_H}{k_l}}\Delta P^{0.5} t^{0.5} \tag{18}$$

Assuming P_p is small relative to P_a and $\Delta P^{0.5}$ becomes $P_a^{0.5}$, so Eqn. 18 becomes

$$n = \sqrt{\frac{2DK_H'}{k_l}} P_a^{0.5} t^{0.5} \quad (19)$$

Equation 19 is of the same form as the integrated empirical rate (Eqn. 10) and the rate constant, d, is equal to $(2DK_H'/k_l)^{0.5}$. The assumption that P_p is small relative to P_a is only true after a sufficient amount of pyrite has oxidized and the film has had time to develop. We found that after approximately 24 h, P_P became small with respect to P_a (<5%). When we discarded all data for measurements before 24 h, we found that value of d (see Eqn. 11) is $6.68(\pm 0.15) \times 10^{-7}$ which is slightly smaller that the value of d ($5.49(\pm 0.13) \times 10^{-7}$) found from the entire data set.

The values of the diffusion constant and the Henry's law constant in thin films are likely to be different than the values of those constants in bulk solution because the properties of water are different (Derjaguin and Churaev, 1986). Using calculated values for d and k_l, we can determine that the apparent value of DK_H' is 1×10^{-16}, which is seven orders of magnitude less than the value of DK_H in bulk, pure water. Inspection of Eqn. 18 shows that no reasonable range of P, t, or k_l, could provide a range of DK_H that could close this gap. The difference may be because diffusion through thin films is much slower than in bulk solution, because oxygen is much less soluble in thin films than bulk solution, or both.

Our model fits oxygen consumption for our experiments quite well (Fig. 9). The model was developed to fit the data after 24 h of reaction, but also does a good job of predicting oxygen consumption at short reaction times.

4.5. Comparison with Other Studies

The initial rates found in this study agree reasonably well with the initial rates of pyrite oxidation in air found by Morth and Smith (1966) (Table 1). Morth and Smith reported that the rate was zero order with respect to time, but inspection of their data, presented in Birle (1963), shows that oxygen consumption slowed in their experiments in a manner similar to ours.

The rates we found using the modified Barcroft apparatus at times longer than 1–10 d approach the rates found using humidity cells, although the humidity cells rates are reported to be zeroth order with respect to time. Humidity cells, which probably represent an average of air oxidation, aqueous oxidation, and oxygen diffusion through gas and liquid filled void spaces, may approximate the rate of oxidation in air after a thick film of aqueous solution develops on the surface of pyrite grains.

4.6. Application of Results

The models by Ritchie (1994), Elberling, et al. (1994), and Elberling and Nicholson (1996) indicate that the rate of pyrite oxidation in the field is limited by oxygen diffusion through the waste pile. Nevertheless, these models require an appropriate expression of the oxidation rate at the pyrite surface. The diffusion models assume that the reaction order of oxygen is first order at low oxygen concentrations. Our results suggest that the reaction order of 0.5 may be more appropriate. However, at low oxygen partial pressures, the difference between $P^{0.5}$ and $P^{1.0}$ may have little effect on the models' predictions.

Our study measures abiotic oxidation rates, but in natural environments microbes could also contribute to the production of acid mine drainage. For example, *Leptospirillum ferrooxidans* have been found in waste piles, and are known to increase the rate of pyrite oxidation (Nordstrom and Southam, 1997; Schrenk et al., 1998). Thin films of solution associated with oxidizing pyrite may provide an environment for *L. ferroxidans* growth even in the absence of a bulk aqueous phase. However, our results suggest that the growth rate of these organisms may is likely to be limited by oxygen diffusion through the aqueous films.

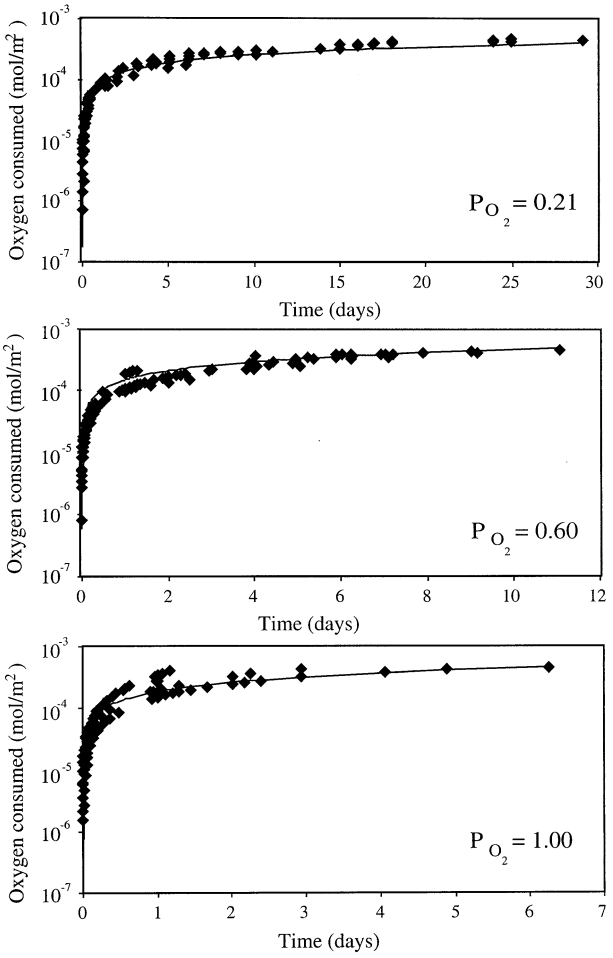

Fig. 9. Comparison of the number of moles of oxygen consumed versus time from our experiments (diamonds) and the amounts predicted by our transport model (lines).

Museum pyrites probably disaggregate due to the precipitation, in surface cracks, of ferrous sulfates, which have a much larger molar volume than pyrite (V_m(pyrite) = 23.94 cm^3/mol; V_m(melanterite) = 146.50 cm^3/mol; V_m(szomolnokite) = 55.90 cm^3/mol; Robie and Hemingway, 1995). We know the solubility of ferrous sulfate in sulfuric acid from Linke (1958) and we can use Pitzer equations to predict the activity of water in equilibrium with these solutions (Pitzer, 1991). Using these two pieces of information, we can determine the activity of water (and thus the relative humidity) of ferrous sulfate + sulfuric acid solutions (Fig. 10). During the initial oxidation stage, pyrite produces equal molar quantities of ferrous sulfate and

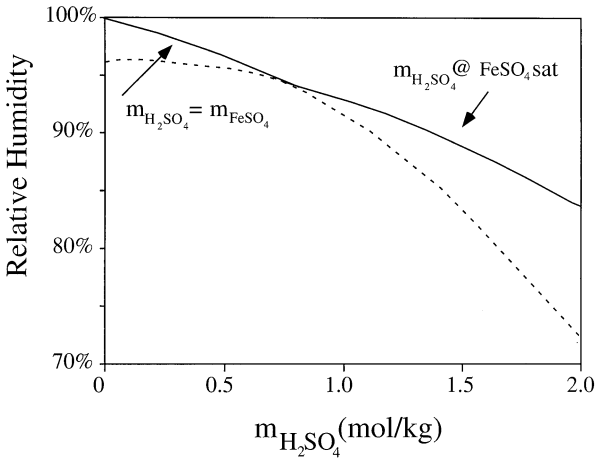

Fig. 10. Graph showing the concentrations in ferrous sulfate + sulfuric acid solutions in equilibrium with a vapor phase with varying relative humidity. At low concentrations of ferrous sulfate-sulfuric acid, relative humidity decreases with the equal molar increase of the ferrous sulfate and sulfuric acid components of the solution. Below approximately 95% relative humidity, a ferrous sulfate solid becomes saturated and further decreases in relative humidity causes solid ferrous sulfate to crystallize while concentration of the sulfuric acid continues to increase.

sulfuric acid and these hygroscopic species absorb water from the surrounding vapor. The concentration of ferrous sulfate and sulfuric acid in the solution film that forms on the pyrite surface depends on relative humidity in the air surrounding the samples. This dependence is shown graphically as the steeper-sloped solid line on Figure 10. At relative humidity between 100 and 95%, the solutions that form are undersaturated with respect to ferrous sulfate phases. Below approximately 95% relative humidity and a molality of approximately 0.6, the solution is saturated with ferrous sulfate solid, which coexists with the solution. According to the solubility studies summarized by Linke (1958), szomolnokite is the stable ferrous sulfate at this acidity, but Borek (1994) reported the occurrence of melanterite and rozenite on the surface of pyrite that oxidized in relative humidity between 70 and 79%, so there may be a kinetic barrier to the formation of szomolnokite. All three ferrous sulfates have a larger molar volume than pyrite and should be capable of widening fractures as they crystallize. Pyrite oxidation at relative humidity below 95% relative humidity produces ferrous sulfate solid and ferrous sulfate + sulfuric acid solutions. The solutions that form at moderate relative humidity (70–80%) becomes quite concentrated in H_2SO_4 and the solubility of ferrous sulfate in these solutions is very low.

The formation of ferrous sulfate salts in cracks or void spaces in and between pyrite grains can wedge the sample apart. In addition, the sulfuric acid can dissolve some of the phases intergrown with the pyrite, leading to disintegration of the entire sample. Our results indicate that at high relative humidity (greater than 96%), the sample may be protected from disaggregation because ferrous sulfate remains undersaturated. The most "dangerous" conditions for pyrite samples is midrange relative humidity where there is sufficient water present to react with pyrite and form a solution on the surface, but not enough to dissolve ferrous sulfate. Because water is a necessary reactant (Eqn. 1) for the oxidation of pyrite, we presume that at some low relative humidity the rate of pyrite oxidation becomes limited by a lack of water.

5. CONCLUSIONS

We have designed and built a reactor to measure the rate of oxygen consumption by pyrite oxidation in humid air. The rate is:

$$\frac{dn}{dt} = 10^{-6.6} P^{0.5} t^{-0.5} \tag{20}$$

The initial rate of oxidation is equal to or greater than the rate of oxidation in solution at the same partial pressure of oxygen, but slows as a ferrous sulfate + sulfuric acid solution film builds on the pyrite surface and the transport of oxygen through this film limits the rate of oxygen delivery to the pyrite surface. At long times the film become so extensive that the pyrite oxidation rate becomes similar to those found in humidity cell studies.

This rate law can be used to predict the behavior of oxidizing pyrite in waste piles, which is an important factor in acid prediction models. In addition, the results of this study suggest humid environments with relative humidity less than 95% can promote the disintegration of museum pyrite samples because ferrous sulfate phases precipitate. At moderate relative humidity (~70%), the solution that develops on oxidizing pyrite surfaces can become very acidic ($m_{H_2SO_4} > 2.0$).

Acknowledgments—Dan Smith made the Barcroft apparatus and stands. The FESEM photomicrographs were collected thanks to the microscopy skills of Rob Weaver. The search for bacteria was performed with the aid of Steven Lower and Treavor Kendall. This manuscript was improved by the suggestions of James Craig, Patricia Dove, Lee Daniels, and D. Kirk Nordstrom. The authors thank Bob Seal and an anonymous reviewer for their comments on the final manuscript. Funding for this project was provided by a grant from the NSF (EAR-0003364), the Waste Policy Institute at Virginia Tech, and the Graduate Student Assembly at Virginia Tech.

Associate editor: M. A. McKibben

REFERENCES

Bannister F. A. (1933) The preservation of pyrites and marcasite. *The Museums J.* **33,** 72–75.

Bannister F. A. (1937) Preservation of minerals and meteorites. *The Museums J.* **36,** 465–476.

Birle H. D. (1963) Sulfide to Sulfate Reaction Mechanism in Pyritic Materials. M.S., The Ohio State University.

Borek S. L. (1994) Effect of humidity on pyrite oxidation. In *Environmental Geochemistry of Sulfide Oxidation, ACS Symp. Series550* (eds. C. N. Alpers and D. W. Blowes), pp. 31–44. American Chemical Society.

Crank J. (1975) *The Mathematics of Diffusion*. Clarendon Press.

Derjaguin B. V. and Churaev N. V. (1886) Properties of water layers adjacent to interfaces. In *Fluid Interfacial Phenomena* (ed. C. A. Croxton), p 663–738. Wiley, New York.

Elberling B. and Nicholson R. V. (1996) Field determination of sulphide oxidation rates in mine tailings. *Water Res. Res.* **32,** *(6),* 1773–1784.

Elberling B., Nicholson R. V., and Scharer J. M. (1994) A combined kinetic and diffusion model of pyrite oxidation in tailings: a change in controls with time. *J. Hydrol.* **157,** 47–60.

Elsetinow A. R., Guevremont J. M., Strongin D. R., Schoonen M. A. A., and Strongin M. (2000) Oxidation of {100} and {111} surfaces of pyrite. Effects of preparation method. *Am. Mineral.* **85,** *(3–4),* 623–626.

Foust A. S., Wenzel L. A., Clump C. W., Maus L., and Andersen L. B. (1980) Principles of Unit Operations. John Wiley & Sons.

Gerhardt P., Murray R. G. E., Wood W. A., and Krieg N. R. (1994) Methods for General and Molecular Bacteriology. p. 791. American Society for Microbiology.

Guevremont J. M., Bebie J., Elsetinow A. R., Strongin D. R., and Schoonen M. A. A. (1998a) Reactivity of the (100) plane of pyrite in oxidizing gaseous and aqueous environments: Effects of surface imperfections. *Env. Sci. Tech.* **32,** 3743–3748.

Guevremont J. M., Strongin D. R., and Schoonen M. A. A. (1998b) Thermal chemistry of H_2S and H_2O on the (001) plane of pyrite: Unique reactivity of defects sites. *Am. Mineral.* **83,** 1246–1255.

Hammack R. W. and Watzlaf G. R. (1990) The effect of oxygen of pyrite oxidation. *Proceedings of the 1990 Mining and Reclamation Conference and Exhibition,* 19–25.

Howie F. M. (1992) Pyrite and marcasite. In *Care and Conservation of Geological Material: Minerals, Rocks, Meteorites and Lunar Finds* (ed. F. M. Howie), pp. 70–84. Butterworth.

Jerz J. K. (2002) Geochemical reactions in unsaturated mine waste. Ph.D. Dissertation, Virginia Polytechnic Institute and State University. <http://scholar.lib.vt.edu/theses/available/etd-04252002-125213/>.

Kelly M. G. (1999) Effects of heavy metals on the aquatic biota. In *The Environmental Geochemistry of Minerals Deposits* (eds. G. S. Plumlee and M. J. Logsdon) Vol. 6A, pp. 363–371. Society of Economic Geologists.

Kim H. W. (1964) The effect of water concentration on vapor phase oxidation of pyrite. M.S. Thesis, The Ohio State University.

Knipe S. W., Mycroft J. R., Pratt A. R., Nesbitt H. W., and Bancroft G. M. (1995) X-ray photoelectron spectroscopic study of water adsorption on iron sulphide minerals. *Geochim. Cosmochim. Acta* **59,** 1079–1090.

Langmuir D. (1997) Aqueous Environmental Geochemistry. Prentice Hall.

Lau C. M., Shumate K. S., and Smith E. E. (1970) The role of bacteria in pyritic oxidation kinetics. *Third Symposium on Coal Mine Drainage Research.* 114–122.

Linke W. F. (1958) Ferrous Sulfate $FeSO_4$. In *Solubilities: Inorganic and Metal-Organic Compounds* Vol. 1, pp. 1046–1053. D. Van Nostrand Company, Inc.

McKibben M. A. and Barnes H. L. (1986) Oxidation of pyrite in low temperature acidic solutions: rate laws and surface textures. *Geochim. Cosmochim. Acta* **50,** 1509–1520.

Morth A. H. and Smith E. E. (1966) Kinetics of the sulfide-to-sulfate reaction. *Am. Chem. Soc. Div. Fuel Chem. Preprints.* **10,** 83.

Nesbitt H. W., Bancroft G. M., Pratt A. R., and Scaini M. J. (1998) Sulfur and iron surface states of fractured pyrite surfaces. *Am. Mineral.* **83,** 1067–1076.

Nesbitt H. W. and Muir I. J. (1994) X-ray photoelectron spectroscopic study of a pristine pyrite surface reacted with water vapour and air. *Geochim. Cosmochim. Acta* **58,** 4667–4679.

Nesbitt H. W., Scaini M., Hoechst H., Bancroft G. M., Schaufuss A. G., and Szargan R. (2000) Synchrotron XPS evidence for Fe(II)-S and Fe(III)-S surface species on pyrite fracture-surfaces, and their 3D electronic states. *Am. Mineral.* **85,** 850–857.

Nicholson R. V., Gillham R. W., and Reardon E. J. (1988) Pyrite oxidation in carbonate-buffered solution. *Geochim. Cosmochim. Acta* **52,** 1077–1085.

Nordstrom D. K. and Southam G. (1997) Geomicrobiology of sulfide mineral oxidation. In *Geomicrobiology: Interactions Between Microbes and Minerals* (eds. J. F. Banfield and K. H. Nealson) Vol. 35, pp. 361–390. Reviews in Mineralogy.

Pitzer K. S. (1991) Ion Interaction Approach: Theory and data correlation. In *Activity Coefficients in Electrolyte Solutions* (ed. K. S. Pitzer), pp. 75–153. CRC Press.

Plumlee G. S. and Logsdon M. J. (1999) The environmental geochemistry of mineral deposits. In *Reviews in Economic Geology* Vol. 6A. Society of Economic Geologists.

Ritchie A. I. M. (1994) Rates of mechanism that govern pollutant generation from pyritic wastes. In *Environmental Geochemistry of Sulfide Oxidation, ACS Symp. Series550* (eds. C. N. Alpers and D. W. Blowes), pp. 108–122. American Chemical Society.

Robie R. A., and Hemingway B. S. (1995) Thermodynamic Properties of Minerals and Related Substances at 298.15 K and 1 Bar (10^5 Pascals) Pressure and at Higher Temperatures. U.S. Geological Survey.

Robinson R. A. and Stokes R. H. (1959) Electrolyte Solutions: The Measurement and Interpretation of Conductance, Chemical Potential and Diffusion in Solutions of Simple Electrolytes. Academic Press Inc., Publishers.

Rogowski A. S., and Pionke H. B. (1984) Hydrology and Water Quality on Strip-mined Lands. U.S. Environmental Protection Agency.

Schrenk M. O., Edwards K. J., Goodman R. M., Hamers R. J., and Banfield J. F. (1998) Distribution of *Thiobacillus ferrooxidans* and *Leptosprillum ferrooxidans*: Implications for generation of acid mine drainage. *Science* **279,** 1519–1522.

Singer P. C. and Stumm W. (1970) Acidic mine drainage: The rate-determining step. *Science* **163,** 1121–123.

Smith K. S. and Huyck H. L. O. (1999) An overview of the abundance, relative mobility, bioavailability, and human toxicity of metals. In *The Environmental Geochemistry of Minerals Deposits* (eds. G. S. Plumlee and M. J. Logsdon) Vol. 6A, pp. 29–70. Society of Economic Geologists.

Staley J. T., Bryant M. P., Pfenning N., and Holt J. G. (1984) Bergey's Manual of Systematic Bacteriology, Vol. 3. Williams & Wilkins, p. 1842–1858.

Todd E. C., Sherman D. M., and Purton J. A. (2003) Surface oxidation of pyrite under ambient atmospheric and aqueous (pH = 2 to 10) conditions: Electronic structure and mineralogy from X-ray absorption spectroscopy. *Geochim. Cosmochim. Acta* **67,** 881–893.

Tromans D. (2000) Modeling oxygen solubility in water and electrolyte solutions. *Indust. Eng. Chem. Res.* **39 (***3***),** 805–812.

Umbreit W. W., Burris R. H., and Stauffer J. F. (1972) *Manometric and Biochemical Techniques*. Burgess Publishing Company.

Williamson M. A. and Rimstidt J. D. (1994) The kinetics and electrochemical rate-determining step of aqueous pyrite oxidation. *Geochim. Cosmochim. Acta* **58,** 5443–5454.

Appendix 1. Data from All Successful Experiments

PY33

t min	n mol	P atm	r mol/m^{2}sec
23	2.97×10^{-7}	0.209	
38	3.71×10^{-7}	0.209	5.14×10^{-9}
103	8.16×10^{-7}	0.208	4.05×10^{-9}
183	1.30×10^{-6}	0.207	3.43×10^{-9}
382	2.15×10^{-6}	0.205	2.05×10^{-9}
856	3.23×10^{-6}	0.202	1.12×10^{-9}
1418	3.97×10^{-6}	0.200	4.33×10^{-10}
1880	3.93×10^{-6}	0.200	9.97×10^{-11}
2122	4.08×10^{-6}	0.200	6.21×10^{-10}
2865	4.82×10^{-6}	0.198	5.77×10^{-10}
4315	5.93×10^{-6}	0.196	4.72×10^{-10}
7187	7.78×10^{-6}	0.191	4.23×10^{-10}
8722	8.97×10^{-6}	0.188	

PY43

t min	n mol	P atm	r mol/m^{2}sec
52	7.33×10^{-8}	0.210	
70	1.10×10^{-7}	0.210	2.60×10^{-9}
125	3.37×10^{-7}	0.209	2.62×10^{-9}
187	5.87×10^{-7}	0.209	2.84×10^{-9}
268	9.53×10^{-7}	0.208	3.11×10^{-9}
304	1.17×10^{-6}	0.207	3.12×10^{-9}
387	1.50×10^{-6}	0.206	2.35×10^{-9}
444	1.69×10^{-6}	0.206	2.46×10^{-9}
684	2.53×10^{-6}	0.204	1.94×10^{-9}
1542	4.51×10^{-6}	0.199	1.30×10^{-9}
1620	4.74×10^{-6}	0.198	1.49×10^{-9}
1942	5.39×10^{-6}	0.197	1.04×10^{-9}
3036	6.82×10^{-6}	0.193	1.01×10^{-9}
3390	7.81×10^{-6}	0.191	1.15×10^{-9}
4483	9.24×10^{-6}	0.187	7.82×10^{-10}
5927	1.08×10^{-5}	0.184	6.69×10^{-10}
7244	1.21×10^{-5}	0.180	5.93×10^{-10}
8943	1.35×10^{-5}	0.177	

PY49

t min	n mol	P atm	r mol/m^{2}sec
6	3.67×10^{-8}	0.210	
10	2.20×10^{-7}	0.209	1.86×10^{-8}
15	2.93×10^{-7}	0.209	6.73×10^{-9}
25	3.67×10^{-7}	0.209	2.56×10^{-9}
33	3.67×10^{-7}	0.209	4.17×10^{-9}
49	5.13×10^{-7}	0.209	5.78×10^{-9}
92	8.43×10^{-7}	0.208	4.78×10^{-9}
131	1.14×10^{-6}	0.207	3.96×10^{-9}
163	1.28×10^{-6}	0.207	3.42×10^{-9}
335	2.05×10^{-6}	0.205	2.24×10^{-9}
452	2.35×10^{-6}	0.204	1.64×10^{-9}
518	2.53×10^{-6}	0.204	1.62×10^{-9}
683	2.90×10^{-6}	0.203	1.41×10^{-9}
1524	4.36×10^{-6}	0.199	9.64×10^{-10}
1715	4.66×10^{-6}	0.199	8.74×10^{-10}
1850	4.80×10^{-6}	0.198	6.99×10^{-10}
2061	5.02×10^{-6}	0.198	6.26×10^{-10}
2868	5.72×10^{-6}	0.196	7.28×10^{-10}
5749	8.65×10^{-6}	0.189	5.96×10^{-10}
6156	9.17×10^{-6}	0.188	4.48×10^{-10}

PY49

t min	n mol	P atm	r mol/m^{2}sec
7231	9.64×10^{-6}	0.186	5.09×10^{-10}
8883	1.13×10^{-5}	0.183	6.69×10^{-10}
10198	1.27×10^{-5}	0.179	5.45×10^{-10}
11608	1.35×10^{-5}	0.177	
13065	1.27×10^{-5}	0.179	
14604	1.33×10^{-5}	0.178	4.36×10^{-10}
15911	1.46×10^{-5}	0.174	3.50×10^{-10}
20017	1.61×10^{-5}	0.171	2.06×10^{-10}
21651	1.65×10^{-5}	0.170	4.74×10^{-10}
23141	1.83×10^{-5}	0.165	8.78×10^{-10}
24427	2.02×10^{-5}	0.161	6.79×10^{-10}
26008	2.13×10^{-5}	0.158	2.31×10^{-10}
34440	2.35×10^{-5}	0.153	2.07×10^{-10}
35945	2.46×10^{-5}	0.150	
41888	2.24×10^{-5}	0.155	

PY50

t min	n mol	P atm	r mol/m^{2}sec
1	4.74×10^{-7}	0.209	
5	7.18×10^{-8}	0.210	
20	7.18×10^{-8}	0.210	
28	7.18×10^{-8}	0.210	2.05×10^{-9}
44	1.44×10^{-7}	0.210	3.50×10^{-9}
87	3.59×10^{-7}	0.209	2.74×10^{-9}
126	5.02×10^{-7}	0.209	2.26×10^{-9}
158	6.10×10^{-7}	0.209	2.96×10^{-9}
330	1.29×10^{-6}	0.207	2.33×10^{-9}
447	1.72×10^{-6}	0.206	2.10×10^{-9}
513	1.90×10^{-6}	0.205	1.90×10^{-9}
678	2.37×10^{-6}	0.204	1.74×10^{-9}
1519	4.16×10^{-6}	0.200	1.18×10^{-9}
1710	4.52×10^{-6}	0.199	1.14×10^{-9}
1845	4.74×10^{-6}	0.198	1.03×10^{-9}
2056	5.06×10^{-6}	0.198	1.07×10^{-9}
4664	8.51×10^{-6}	0.189	8.35×10^{-10}
5744	1.04×10^{-5}	0.185	6.41×10^{-10}
6151	1.00×10^{-5}	0.186	2.27×10^{-10}
7226	1.09×10^{-5}	0.183	5.50×10^{-10}
8878	1.23×10^{-5}	0.180	5.54×10^{-10}
10193	1.34×10^{-5}	0.177	4.82×10^{-10}
11603	1.43×10^{-5}	0.175	3.43×10^{-10}
13060	1.49×10^{-5}	0.174	2.90×10^{-10}
14599	1.56×10^{-5}	0.172	3.31×10^{-10}
21646	1.89×10^{-5}	0.164	2.68×10^{-10}
23136	1.94×10^{-5}	0.163	1.94×10^{-10}
24422	1.98×10^{-5}	0.162	2.13×10^{-10}
26003	2.03×10^{-5}	0.160	1.17×10^{-10}
34435	2.15×10^{-5}	0.158	9.37×10^{-11}
35940	2.18×10^{-5}	0.157	1.36×10^{-10}
41883	2.30×10^{-5}	0.154	

PY36

t min	n mol	P atm	r mol/m^{2}sec
3	2.72×10^{-7}	0.599	
5	4.27×10^{-7}	0.599	2.67×10^{-8}
13	6.13×10^{-7}	0.599	9.46×10^{-9}
50	9.32×10^{-7}	0.598	4.41×10^{-9}

(continued)

Appendix 1. (Continued)

PY36

t min	n mol	P atm	r mol/m^{2}sec
88	1.16×10^{-6}	0.597	4.42×10^{-9}
122	1.44×10^{-6}	0.596	4.72×10^{-9}
210	1.98×10^{-6}	0.595	3.72×10^{-9}
311	2.52×10^{-6}	0.594	3.28×10^{-9}
453	3.18×10^{-6}	0.592	4.02×10^{-9}
696	4.81×10^{-6}	0.588	2.05×10^{-9}
843	4.47×10^{-6}	0.589	5.83×10^{-10}
1438	5.41×10^{-6}	0.587	7.98×10^{-10}
1663	5.55×10^{-6}	0.586	3.72×10^{-10}
1815	5.63×10^{-6}	0.586	4.29×10^{-10}
2278	5.94×10^{-6}	0.586	8.23×10^{-10}
2886	6.97×10^{-6}	0.583	8.32×10^{-10}
3597	7.62×10^{-6}	0.581	1.08×10^{-9}
5758	1.14×10^{-5}	0.572	7.74×10^{-10}
7298	1.22×10^{-5}	0.570	

PY37

t min	n mol	P atm	r mol/m^{2}sec
33	8.18×10^{-7}	0.598	
132	1.36×10^{-6}	0.597	7.68×10^{-9}
1472	9.63×10^{-6}	0.577	2.59×10^{-9}
1603	1.00×10^{-5}	0.576	1.83×10^{-9}
1715	1.03×10^{-5}	0.575	1.71×10^{-9}
1829	1.06×10^{-5}	0.574	8.82×10^{-10}
5607	1.42×10^{-5}	0.565	9.97×10^{-10}
5803	1.83×10^{-5}	0.555	1.18×10^{-9}
7135	1.68×10^{-5}	0.559	2.52×10^{-10}
8507	1.93×10^{-5}	0.553	1.00×10^{-9}
8981	1.97×10^{-5}	0.552	
9978	1.93×10^{-5}	0.553	2.23×10^{-10}
11404	2.05×10^{-5}	0.550	2.52×10^{-10}
13172	2.05×10^{-5}	0.550	

PY38

t min	n mol	P atm	r mol/m^{2}sec
2	4.14×10^{-8}	0.600	
112	7.45×10^{-7}	0.598	3.00×10^{-9}
281	1.53×10^{-6}	0.596	2.98×10^{-9}
1440	4.92×10^{-6}	0.588	1.51×10^{-9}
2818	7.90×10^{-6}	0.581	1.26×10^{-9}
3290	8.90×10^{-6}	0.578	8.30×10^{-10}
5490	1.10×10^{-5}	0.573	1.18×10^{-9}
5713	1.38×10^{-5}	0.566	2.08×10^{-9}
7522	1.70×10^{-5}	0.558	1.23×10^{-9}
8687	1.95×10^{-5}	0.552	

PY40

t min	n mol	P atm	r mol/m^{2}sec
4	1.41×10^{-7}	0.600	
6.5	1.76×10^{-7}	0.600	7.40×10^{-9}
12	2.25×10^{-7}	0.599	7.48×10^{-9}
32	4.22×10^{-7}	0.599	6.90×10^{-9}
65	7.75×10^{-7}	0.598	5.80×10^{-9}
128	1.23×10^{-6}	0.597	4.08×10^{-9}
219	1.73×10^{-6}	0.596	3.22×10^{-9}
381	2.43×10^{-6}	0.594	2.46×10^{-9}
811	3.73×10^{-6}	0.591	1.77×10^{-9}
1260	4.89×10^{-6}	0.588	1.51×10^{-9}
1694	5.81×10^{-6}	0.586	1.45×10^{-9}

PY40

t min	n mol	P atm	r mol/m^{2}sec
1949	6.48×10^{-6}	0.584	1.51×10^{-9}
2690	7.99×10^{-6}	0.581	1.36×10^{-9}
4337	1.12×10^{-5}	0.573	1.23×10^{-9}
6371	1.49×10^{-5}	0.564	1.07×10^{-9}
7132	1.60×10^{-5}	0.561	9.42×10^{-10}
7730	1.69×10^{-5}	0.559	8.30×10^{-10}
8496	1.77×10^{-5}	0.557	6.08×10^{-10}
9045	1.81×10^{-5}	0.556	4.87×10^{-10}
10126	1.89×10^{-5}	0.554	6.00×10^{-10}
10397	1.94×10^{-5}	0.553	6.37×10^{-10}
11375	2.01×10^{-5}	0.551	5.59×10^{-10}
12978	2.16×10^{-5}	0.547	

PY53

t min	n mol	P atm	r mol/m^{2}sec
7	1.81×10^{-7}	0.600	
10	2.53×10^{-7}	0.599	1.02×10^{-8}
40	5.42×10^{-7}	0.599	3.96×10^{-9}
62	6.15×10^{-7}	0.599	5.05×10^{-9}
81	8.68×10^{-7}	0.598	5.77×10^{-9}
103	9.76×10^{-7}	0.598	2.55×10^{-9}
160	1.16×10^{-6}	0.597	2.39×10^{-9}
220	1.41×10^{-6}	0.597	2.83×10^{-9}
304	1.77×10^{-6}	0.596	2.89×10^{-9}
390	2.17×10^{-6}	0.595	2.88×10^{-9}
452	2.44×10^{-6}	0.594	2.73×10^{-9}
520	2.71×10^{-6}	0.593	2.47×10^{-9}
687	3.29×10^{-6}	0.592	2.22×10^{-9}
1324	5.13×10^{-6}	0.587	1.63×10^{-9}
1440	5.42×10^{-6}	0.587	1.57×10^{-9}
1612	5.82×10^{-6}	0.586	1.45×10^{-9}
1730	6.07×10^{-6}	0.585	1.33×10^{-9}
1861	6.33×10^{-6}	0.585	1.35×10^{-9}
2084	6.80×10^{-6}	0.583	1.42×10^{-9}
2418	7.52×10^{-6}	0.582	1.33×10^{-9}
2893	8.42×10^{-6}	0.579	1.18×10^{-9}
3122	8.82×10^{-6}	0.578	1.19×10^{-9}
3454	9.44×10^{-6}	0.577	1.12×10^{-9}
4230	1.07×10^{-5}	0.574	9.58×10^{-10}
5867	1.28×10^{-5}	0.569	8.25×10^{-10}
6221	1.33×10^{-5}	0.567	7.97×10^{-10}
7044	1.42×10^{-5}	0.565	7.37×10^{-10}
9011	1.64×10^{-5}	0.560	6.74×10^{-10}
10222	1.76×10^{-5}	0.557	6.99×10^{-10}
15918	2.31×10^{-5}	0.544	

PY27

t min	n mol	P atm	r mol/m^{2}sec
2	1.12×10^{-7}	1.000	
5	1.86×10^{-7}	1.000	1.55×10^{-8}
10	2.98×10^{-7}	0.999	1.64×10^{-8}
15	4.46×10^{-7}	0.999	1.46×10^{-8}
26	6.32×10^{-7}	0.998	9.46×10^{-9}
29	6.69×10^{-7}	0.998	1.24×10^{-8}
43	9.30×10^{-7}	0.998	1.49×10^{-8}
132	2.49×10^{-6}	0.994	9.03×10^{-9}
169	2.98×10^{-6}	0.993	1.01×10^{-8}
281	4.61×10^{-6}	0.989	9.60×10^{-9}
629	8.93×10^{-6}	0.978	7.08×10^{-9}
816	1.10×10^{-5}	0.973	7.60×10^{-9}
1449	1.76×10^{-5}	0.957	5.94×10^{-9}
1544	1.84×10^{-5}	0.955	

(continued)

Appendix 1. (Continued)

PY31

t min	n mol	P atm	r mol/m^{2}sec
4	7.86×10^{-8}	1.000	
34	7.07×10^{-7}	0.998	1.13×10^{-8}
85	1.53×10^{-6}	0.996	1.08×10^{-8}
138	2.51×10^{-6}	0.994	1.10×10^{-8}
204	3.53×10^{-6}	0.991	9.72×10^{-9}
356	5.54×10^{-6}	0.986	7.73×10^{-9}
466	6.79×10^{-6}	0.983	9.41×10^{-9}
888	1.23×10^{-5}	0.970	5.06×10^{-9}
1406	1.41×10^{-5}	0.966	2.40×10^{-9}
1449	1.46×10^{-5}	0.964	

PY41

t min	n mol	P atm	r mol/m^{2}sec
3	8.89×10^{-7}	0.998	
9	3.23×10^{-7}	0.999	
20	5.25×10^{-7}	0.999	8.60×10^{-9}
33	6.46×10^{-7}	0.998	3.77×10^{-8}
24	8.08×10^{-7}	0.998	6.20×10^{-9}
85	9.69×10^{-7}	0.998	2.31×10^{-9}
97	1.13×10^{-6}	0.997	8.00×10^{-9}
158	1.78×10^{-6}	0.996	6.44×10^{-9}
268	2.75×10^{-6}	0.993	5.51×10^{-9}
378	3.68×10^{-6}	0.991	5.31×10^{-9}
524	4.81×10^{-6}	0.988	5.05×10^{-9}
1297	9.53×10^{-6}	0.977	3.23×10^{-9}
1375	9.86×10^{-6}	0.976	3.31×10^{-9}
1498	1.05×10^{-5}	0.974	3.54×10^{-9}
1846	1.23×10^{-5}	0.970	3.34×10^{-9}
2901	1.72×10^{-5}	0.958	2.73×10^{-9}
3244	1.86×10^{-5}	0.955	2.70×10^{-9}
4215	2.24×10^{-5}	0.945	

PY54

t min	n mol	P atm	r mol/m^{2}sec
18	1.40×10^{-7}	1.000	
35	2.44×10^{-7}	0.999	4.66×10^{-9}
57	4.19×10^{-7}	0.999	5.93×10^{-9}
76	6.28×10^{-7}	0.998	6.68×10^{-9}
98	8.38×10^{-7}	0.998	5.87×10^{-9}
155	1.29×10^{-6}	0.997	5.00×10^{-9}
215	1.75×10^{-6}	0.996	4.66×10^{-9}
299	2.30×10^{-6}	0.994	4.12×10^{-9}
385	2.83×10^{-6}	0.993	3.92×10^{-9}
447	3.21×10^{-6}	0.992	3.86×10^{-9}
515	3.59×10^{-6}	0.991	3.64×10^{-9}
682	4.47×10^{-6}	0.989	3.43×10^{-9}
1319	7.33×10^{-6}	0.982	2.54×10^{-9}
1435	7.78×10^{-6}	0.981	2.64×10^{-9}
1607	8.48×10^{-6}	0.979	2.49×10^{-9}
1725	8.90×10^{-6}	0.978	2.48×10^{-9}
1856	9.42×10^{-6}	0.977	2.48×10^{-9}
2079	1.02×10^{-5}	0.975	2.48×10^{-9}
2413	1.15×10^{-5}	0.972	2.17×10^{-9}
2888	1.29×10^{-5}	0.969	1.90×10^{-9}
3117	1.36×10^{-5}	0.967	2.05×10^{-9}
3449	1.46×10^{-5}	0.964	1.80×10^{-9}
4225	1.66×10^{-5}	0.960	1.55×10^{-9}
5862	2.01×10^{-5}	0.951	1.36×10^{-9}
7039	2.26×10^{-5}	0.945	8.16×10^{-10}
9006	2.40×10^{-5}	0.941	